

Hyperspectral imaging for thermal analysis and remote gas sensing in the short wave infrared

M. Pisani · P. Bianco · M. Zucco

Received: 5 October 2011 / Published online: 28 April 2012
© Springer-Verlag 2012

Abstract A novel hyperspectral imaging device based on Fourier transform analysis applied to a low finesse scanning Fabry–Pérot (F–P) interferometer has been demonstrated in the short wave infrared (SWIR) region. The technique allows the realization of a lightweight and compact instrument yet allowing much faster and/or better quality hyperspectral images with respect to classical instruments based on a dispersive means or on a tunable band-pass filter. The potentialities in spectroscopic applications like remote gas sensing are presented as well as accurate thermal imaging capabilities.

1 Introduction

Hyperspectral imaging (HI) is a powerful method of analysis which consists in generating the spectral content of each pixel of a two dimensional image. Therefore a HI device is usually made of an imaging device (a digital camera) and a spectrophotometer, and the obtained data set is a 3D matrix, also known as “hyperspectral cube”, where the third dimension is the spectral distribution.

The development of HI devices is growing steadily thanks to the growing number of applications in different fields, for example, just considering the infrared region, these devices are good candidates for thermal imaging, spectroscopy for remote gas sensing, airborne and spaceborne Earth survey and so on.

Classical HI devices are made by integrating a dispersive means (a prism or a grating) or a tunable band-pass filter in

an optical system. Although they have a good image quality and spectral resolution, these devices have a low efficiency in terms of photon collection, which means long integration times. A comprehensive overview on classic HI devices can be found in [1].

The spectral content of the image of a light source can be obtained also by applying the Fourier transform (FT) to the interferogram acquired by a scanning interferometer. This is usually done in the so-called Fourier transform infrared spectroscopy (FTIR). The advantage of having HI devices based on an interferometer is a much higher efficiency with respect to HI devices based on dispersive means. This is due to the Fellgett or multiplex advantage and the Jacquinot or throughput advantage [2, 3]. Promising results using Michelson or Sagnac interferometers are presented in [4, 5]. An alternative method to extract the spectral content of an image employing time-domain processing instead of the frequency-domain analysis in a Michelson interferometer is presented in [6].

A novel HI device based on the use of low finesse Fabry–Pérot interferometer has been described in [7] and its application in the visible region has been demonstrated. Here we present the evolution of the latter in the short wave infrared (SWIR, 900–1750 nm) and the results obtained in thermal imaging and spectroscopic analysis.

2 Working principle

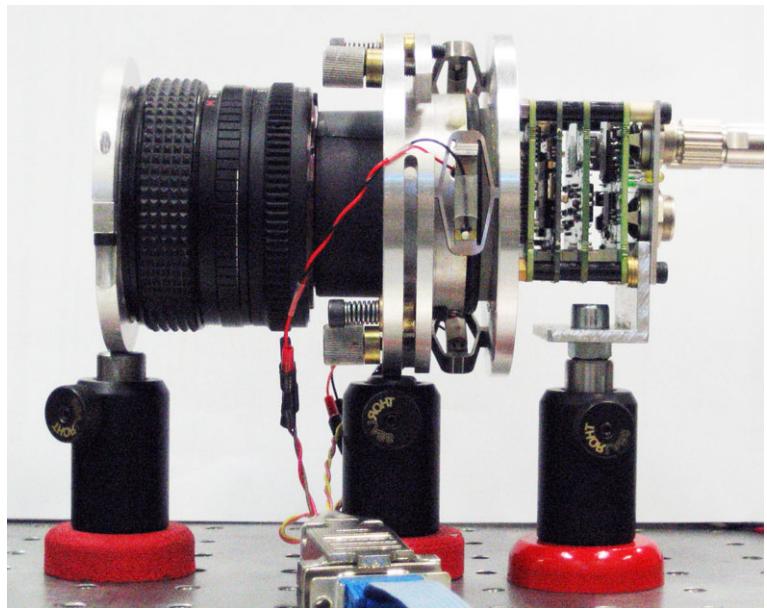
Here is a summary of the theoretical principle and a brief description of the realized F–P cavity.

2.1 Theory

The Fabry–Pérot interferometer is formed by a cavity with two partial reflecting mirrors where d is the distance be-

M. Pisani (✉) · P. Bianco · M. Zucco
Istituto Nazionale di Ricerca Metrologica, INRiM, Strada delle
cacce 73, 10135 Turin, Italy
e-mail: m.pisani@inrim.it

Fig. 1 Picture of the HI device. From the left the photographic objective, the F-P interferometer and the InGaAs CCD camera



tween the mirrors. The Airy function gives the irradiance transmitted by the cavity when illuminated by a monochromatic radiation

$$I_t \propto \frac{1}{1 + \frac{4R}{(1-R)^2} \sin^2\left(\frac{2\pi d}{\lambda}\right)} \quad (1)$$

where R is the reflectivity of the mirrors and λ is the wavelength. Comparing the interferogram of the Fabry–Pérot interferometer in (1) with the interferogram of the Michelson interferometer [4], given by a cosine, it is evident that both interferograms are formed by fringes having the same periodicity, but for the former one the fringes get more pronounced at the increasing of R . When R is sufficiently small (below 30 %) the Fabry–Pérot interferogram approaches a cosine and it is possible to apply an algorithm based on the Fourier transform to calculate the spectrum [6]. The same algorithm could also be used to calculate the spectrum of a broad band source provided that two conditions are met: first, the spectrum of the source should be smaller than an octave in order to discriminate the fundamental spectrum from the second harmonic spectrum generated by the Fourier transform. Second, the number of sampled points per fringe has to be high enough to minimize the contribution of the aliases on the fundamental spectrum. Moreover, the FT algorithm requires the sampling of the interferogram at the position $d = 0$; since this fact is impossible due to the penetration depth of the mirror coating a mathematical reconstruction has been realized to overcome this limitation [3].

2.2 The F–P interferometer

The core of the HI device is the scanning F–P interferometer, shown in Fig. 1. It is made by two mirrors coated with a thin

aluminum layer with a reflectivity around 25 % and mounted in aluminum frames. Three piezo actuators placed on the aluminum frames allow the scan of the cavity pushing the mirrors from a maximum distance of tens of micrometers up to physical contact. A system made by three elastic hinges and three screws allows the optimal alignment and working distance of the mirrors to be found.

3 The experimental realization

In this section it is described the evolution of the HI device presented in [7] and the experimental set-up realized to obtain the results presented in Sect. 4.

3.1 The HI device

The HI device is made of three main elements: a photographic objective, a F–P interferometer and a digital camera. The photographic objective and the camera can be changed according to the applications and to the spectral region considered. In the present realization the mirror distance is varied from zero (contact between mirrors) to a maximum distance which is about 40 μm . The Full Width Half maximum (FWHM) obtained with this scan length is about 20 nm at 1064 nm. A picture of the HI device is presented in Fig. 1.

A video is recorded while the cavity length is scanned. Each pixel of the video is then processed to obtain an interferogram from which it is possible to calculate the spectral distribution of the same by applying a Fourier transform-based algorithm.

Fig. 2 Schematic layout of the experiment. The radiation emitted by the source is collected by the CCD camera passing through the objective and the F–P cavity. In front of the objective is placed the beam splitter on which is sent the reference laser for the calibration

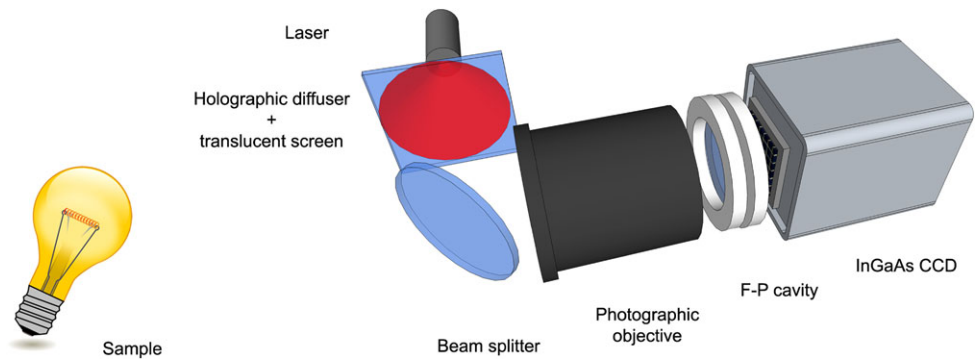
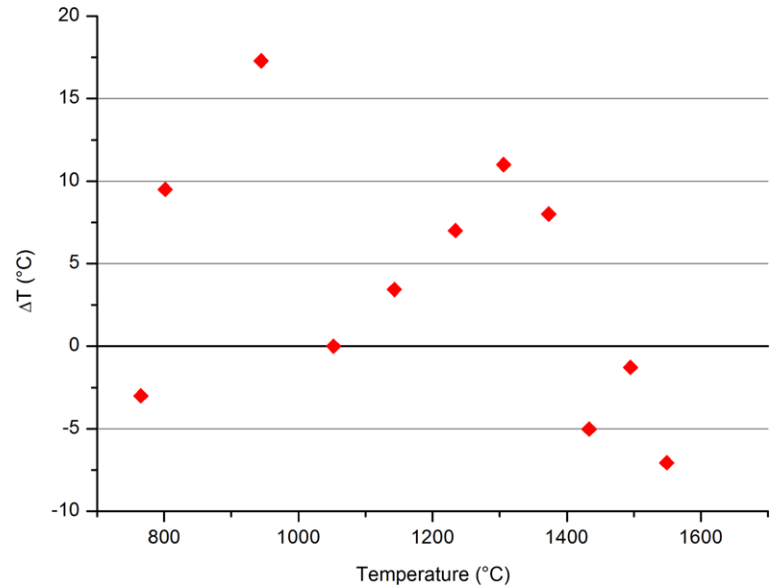


Fig. 3 Absolute temperature measurement errors calculated comparing the temperature measured with a calibrated pyrometer and the temperature estimated from the spectrum measured with the HI device for a tungsten strip lamp used for radiometric measurements



3.2 Experimental set-up

FT analysis requires the knowledge of the position of the sampled point; therefore, it is necessary to know exactly the distance between the mirrors for each frame of the video for each pixel of the image. This is done by analyzing the interferogram of a monochromatic light (a laser), used as a reference for the calibration, from which it is possible to obtain the optical path difference (OPD) of the interferometer.

The schematic layout of the experimental set-up realized is presented in Fig. 2. A diode laser working at 980 nm, used as a reference for SWIR applications, is sent to a holographic diffuser and then projected onto a translucent screen positioned close to a beam splitter fixed in front of the photographic objective. The beam splitter superimposes the image of the screen and the image of the sample.

The camera is a 14-bit InGaAs CCD (Xenics XS-1.7-320) that covers the infrared spectral region from 900 nm up to 1750 nm, placed as close as possible to the F–P interferometer.

In the present realization, two videos have been recorded consequently: the first with the sample superimposed to the

monochromatic light and the second with the sample alone (laser switched off). The frames of the two videos were triggered in such a way that they are synchronous with the mirror distance scan. The same set-up allows one to generate a single video with alternated frames with the laser on and off obtaining similar results.

4 Result and discussion

The SWIR region is of particular interest for the presence of absorption spectra of chemical substances and because in this spectral region there is an important portion of the black-body radiation.

4.1 Temperature estimation

To test the thermal imaging capabilities of the HI device a tungsten strip lamp, normally part of an equipment for radiometric measurements, is used as a variable temperature target. A current controlled power supply is employed to

control the filament temperature that is measured by means of a calibrated pyrometer.

For each temperature measured with the pyrometer at the center of the strip we have acquired a spectrum with the HI device in the same region. In order to correct the measured spectra for the unknown spectral responsivity of the optical system and of the InGaAs CCD camera, we have divided the measured spectrum at $T = 1053\text{ }^\circ\text{C}$ by the Planck black-body function at the same temperature corrected for the tungsten emissivity. Then we have applied this normalization to the remaining spectra. Finally we have fitted every corrected spectrum with the Planck black-body function, thus obtaining the best estimation of the temperature.

The relative errors calculated for each of the temperatures are shown in Fig. 3. The errors are calculated as the difference between the temperature measured with the pyrometer and the temperature estimated with the model described above. The error is within a few degrees Celsius over a temperature range exceeding $1000\text{ }^\circ\text{C}$. It must be noted that the

errors associated to low-temperature measurements can be partially due to the limits of the pyrometric measurements in low irradiance conditions.

4.2 Thermal imaging

By applying the technique described in Sect. 3.1 to each pixel of the surface it is possible to obtain the corresponding temperature and map the surface with the estimated temperature. As an example, we present in Fig. 4 a thermal image of the lower part of the strip lamp described before. The temperature gradient from the bottom to the top is clearly visible in the picture in the middle and it is correctly represented in the thermal image on the right.

In another application we have demonstrated that temperature measurement, estimated through the fit of the black-body function, has reduced dependence on the irradiance of the surface. We have used as a sample a hot metal plate covered with three different materials having different emissivity. This is visible in Fig. 5(a) where the irradiance of the hot plate is represented: the darker region is an aluminum foil placed on the surface, the lighter is cast iron and the remaining region is covered by chalk powder (CaCO_3); the cylindrical element in the middle is a piece of chalk. Looking at its thermal image, Fig. 5(b), it is seen that the estimated temperature, as expected, is rather uniform over the surface.

4.3 Remote gas sensing

We were interested in recognition of chemical substances in the atmosphere by observing absorption bands in the measured spectrum. For this application we have carried out two different experiments: in the first one we have used a halogen lamp as a black-body source, in the second one the Sun.

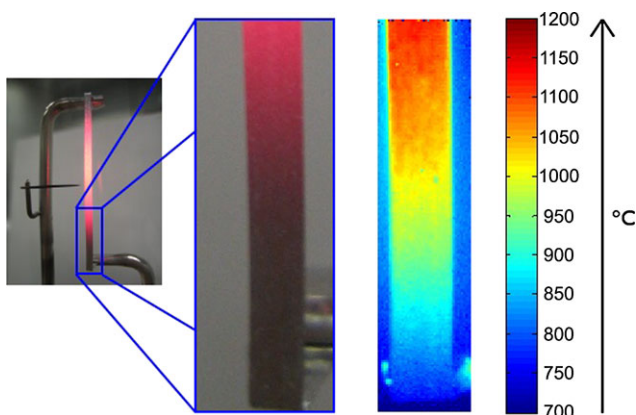


Fig. 4 Thermal imaging of the tungsten strip lamp, for each pixel the temperature of the emitting surface has been estimated

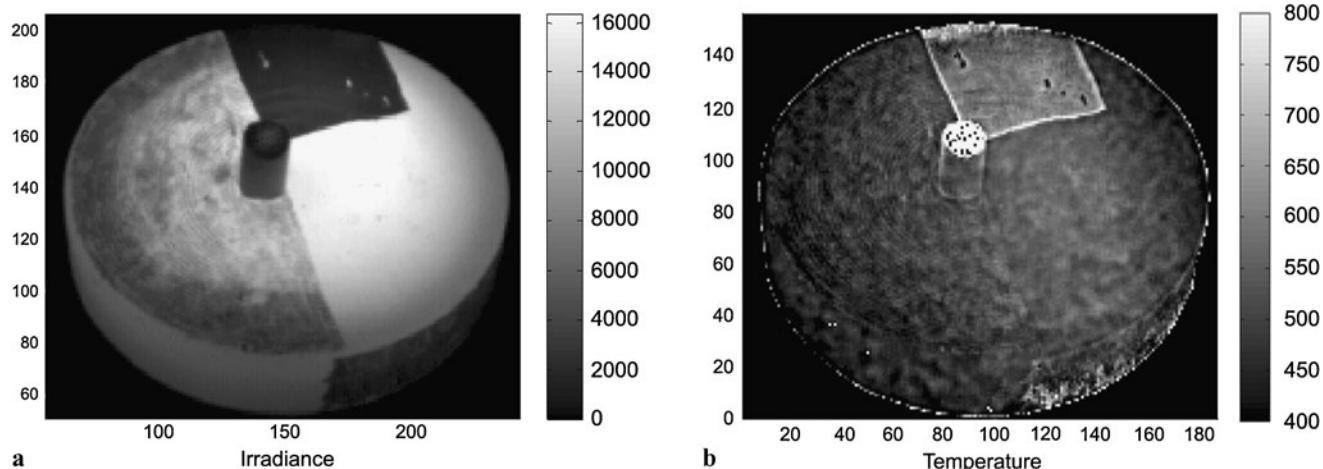


Fig. 5 (a) Irradiance distribution of a hot plate covered by three different materials having different emissivity; (b) thermal image of such hot plate. The temperature does not depend on the irradiance

Fig. 6 Absorption bands of the water in the atmosphere observed in the measured spectra of a halogen lamp at a distance of 3.5 m (black) and 75 m (red)

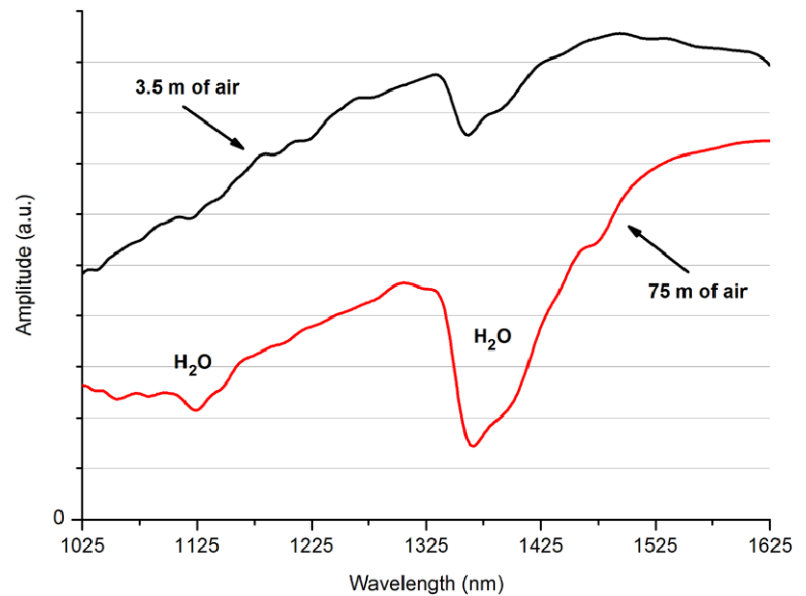
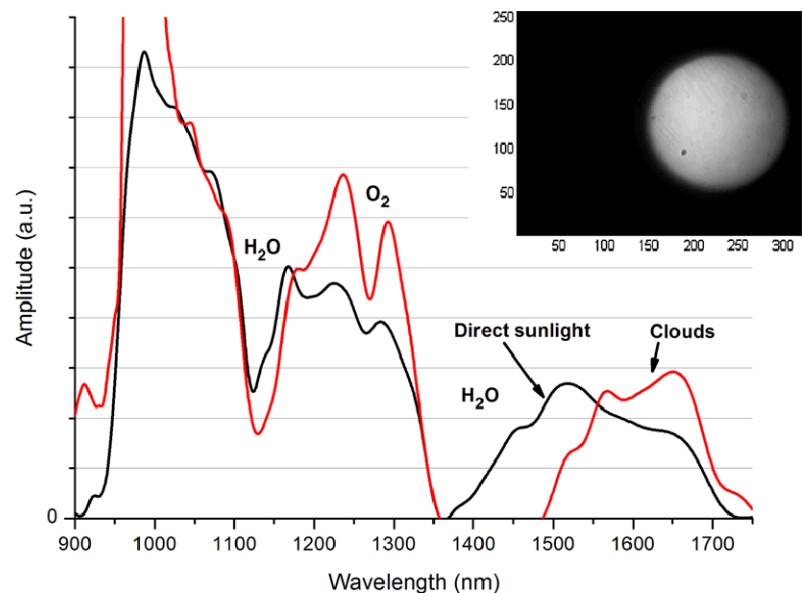


Fig. 7 Spectrum of the sun surface (black) and of the sunlight observed through a cloudy sky (red). Absorption bands of water and oxygen can be observed. At the top right a frame of the video used to obtain the black spectrum



In the first experiment, we placed the lamp at two different distances from the HI device: 3.5 m and 75 m. To perform the measurement at the greater distance it has been necessary to change the photographic objective of the instrument. In Fig. 6 are presented the measured spectra where the absorption bands of the water contained in the air are clearly visible, proportionally increasing with distance.

In the second experiment we have observed the radiation of the sun through the Earth atmosphere. The set-up has been modified by changing the photographic objective with a lens having 1000 mm focal length. Furthermore, in order to compensate the apparent motion of the sun it has been necessary to place the system on a rotating platform during the acquisition.

In a first experiment we have observed the sunlight through a cloudy sky. It is evident the strong absorption in the water bands due to the high concentration of water vapor in the atmosphere (red curve of Fig. 7). In a second experiment we have observed directly the spectrum of the surface of the sun (black curve of Fig. 7). A metalized Mylar sheet has been placed in front of the objective to attenuate the sun light by a 99 %.

5 Conclusions

In this paper, we have presented an hyperspectral imaging (HI) device based on a scanning low finesse F-P cavity operating in the SWIR region (900–1750 nm). The device has

a spectral resolution of 20 nm (FWHM) at 1064 nm and a spatial resolution of 320×256 pixels.

The obtained results highlight the capabilities of the HI device for thermal imaging and remote gas sensing.

The ability to integrate the reference laser used for the calibration makes the instrument compact and suitable for the analysis of subjects at different distances simply using the appropriate objective. Furthermore, it has been demonstrated that the scanning F–P interferometer can be used in different regions of the electromagnetic spectrum simply by changing the sensor of the camera.

The results presented here and in [7] show the potentiality of the device as a compact and lightweight instrument, with high photon collecting efficiency, which make the instrument suitable for airborne or spaceborne applications like Earth survey for security and environmental monitoring.

Further results can be found in [8].

Acknowledgements The authors would like to thank Ferruccio Girard for the calibrated pyrometer and the tungsten strip lamp used to carry out the presented experiments.

References

1. R.G. Sellar, G.D. Boreman, *Opt. Eng.* **44**, 013602 (2005)
2. P.R. Griffiths, J.A. de Haseth, *Fourier Transform Infrared Spectroscopy* (Wiley-Interscience, New York, 2007)
3. M. Pisani, M. Zucco, *Fourier Transforms—Approach to Scientific Principles* (InTech, Rijeka, 2011), Chap. 21
4. R.D. Alcock, J.M. Coupland, *Meas. Sci. Technol.* **17**, 2861 (2006)
5. A. Barducci, P. Marcoionni, I. Pippi, *Ann. Geophys.* **49**, 103 (2006)
6. Y. Jiao, S.R. Bhalotra, H.L. Kung, D.A.B. Miller, *Opt. Express* **11**, 1960 (2003)
7. M. Pisani, M. Zucco, *Opt. Express* **17**, 8319 (2009)
8. http://www.inrim.it/res/hyperspectral_imaging